Real-time measurement system for overlapping reflection signals of fiber Bragg gratings using high-speed wavelength-swept laser

Tatsuya Yamaguchi,[a,*] **Akira Nakamoto**,[b] **and Yukitaka Shinoda**[a]
[a]Nihon University, College of Science and Technology, Department of Electrical Engineering, Tokyo, Japan
[b]Nihon University, Graduate School of Science and Technology, Department of Electrical Engineering, Tokyo, Japan

Abstract. We propose a real-time measurement system that prevents overlapping reflection signals in fiber Bragg gratings (FBGs). The system combines a wavelength-swept laser using Fourier domain mode-locking (FDML) and a buffer stage with three optical paths to obtain a high-speed measurement rate of 304.2 kHz. Systems using high-speed wavelength-swept lasers are affected by the propagation time (delay) of the optical fiber. The delay causes problems such as inaccurate measurements, difficulty in distinguishing FBG reflection signals, and overlapping FBG reflection signals. To prevent these problems, we introduce a method for pulse modulation of a wavelength-swept laser by a fiber switch. This method allows for correction of delays by extracting and identifying only the reflection signal of the FBG at a specific wavelength. By identifying the reflection signals of all FBGs, the overlapping signals can be determined. Accordingly, we devise a measurement method that uses a fiber switch to shade light in the wavelength region of one FBG with overlapping signals from the wavelength-swept light of the laser. This method suppresses overlapping and allows only the reflection signal of the other FBGs to be extracted and demodulated. The proposed system uses bidirectional forward and backward scans with the wavelength-swept laser, such that the shaded FBG signals can be demodulated with either scanning direction. We demonstrate that the system using a three-buffered FDML laser can simultaneously measure the strain or vibration of FBGs installed at arbitrary distances. [DOI: 10.1117/1.OE.61.7.076114]

Keywords: fiber optic sensors; fiber lasers; tunable lasers; optical systems.

Paper 20220465G received May 2, 2022; accepted for publication Jul. 18, 2022; published online Jul. 29, 2022.

1 Introduction

Optical fiber sensors have proven to be a powerful tool for measuring the state of materials and structures with high speed and sensitivity.[1–5] The use of light scattering, interference, modulation, and multicore fibers can improve the performance of optical fiber sensors.[6–14] The fiber Bragg grating (FBG) is a point-type strain and vibration optical sensor widely used in science and engineering because it is easier to manufacture and better adapts to various measurement conditions than other optical fiber sensors.[4,5] Structural health monitoring for qualitative damage assessment through acoustic imaging and high-speed measurement of vibrations exceeding several tens of kilohertz has been reported.[15–21]

In addition, FBGs have drawn attention as ultrasonic receivers for their diverse applications, including underwater applications and structural defect detection.[15–21] For FBGs to function as ultrasonic receivers, the development of a high-speed measurement system that interrogates multiple FBGs is necessary. For the purpose, a system with a simple combination of a wavelength-swept laser and an optical detector can be configured. This system can perform a high-speed measurement of multiple FBGs simultaneously.[22–28] Further speeding up the wavelength-swept lasers leads

*Address all correspondence to Tatsuya Yamaguchi, yamaguchi.tatsuya@nihon-u.ac.jp

to a measurement system for broadband ultrasonic receivers. The measurement rate is determined by the sweep rate of the laser. Recently, buffered Fourier domain mode-locked (FDML) lasers, which use an optical system called a buffer stage to sweep wavelengths multiple times, have been devised to further increase the sweep rate.[29–31] This type of laser has been used as a light source in medicine to achieve the highest imaging speed in optical coherence tomography.[32] To measure FBGs installed at a short distance, we have used a two-buffered FDML laser at a measurement rate of 202.8 kHz.[33]

However, measurements using high-speed wavelength-swept lasers are affected by the propagation time (delay) of the optical fiber that relays the measurement system and FBG. In fact, the delay reduces the measurement accuracy of FBGs. Thus, delay compensation has been developed using optical frequency combs,[34] fiber Fabry–Perot (FFP) etalons,[35] and bidirectional laser scanning.[33,36] On the other hand, for distant FBGs, their reflection signals are folded back within the laser sweep period, hindering their identification. Methods for modulation of the laser sweep frequency[37] and pulse modulation of the laser swept light[38] have been reported for identification. However, no study is available on identification methods for buffered FDML laser, and high-speed measurements have not been achieved using this laser. Furthermore, when FBGs are placed at arbitrary distances, their reflection signals are close together, causing overlapping. Overlapping FBG reflection signals are difficult to identify and demodulate. Very few methods are available to handle this problem in wavelength-swept lasers. Therefore, the wavelength and installation distance of FBGs can be properly selected to avoid overlapping, but this limits the measurement flexibility. Furthermore, as multiplexing of FBGs allows increasing the sensor density, solving overlapping becomes essential.

In recent years, advanced and innovative research on demodulation of overlapping signals has been conducted, resulting in methods using genetic algorithms, search trees, machine learning, deep learning, and other techniques.[39–42] In addition, training data of ideal reflection signals of FBGs have been generated through simulations to validate the developed methods. Although many experimental verifications are expected in the future, fundamental calculations can take several milliseconds for computation, even for fast algorithms, possibly impeding real-time operation.

We propose a measurement system using a three-buffered FDML laser for high-speed real-time measurement of overlapping FBG reflection signals. The laser sweep rate is 304.2 kHz with a bandwidth of 28 nm. In addition, the system uses pulse modulation of swept laser light to identify the reflection signals of FBGs at arbitrary distances. The identification results of the FBG reflection signals are used to determine overlapping. If overlapping between two FBGs is identified, light in the wavelength region of one overlapping FBG is shaded by a fiber switch (FSW) from the wavelength-swept laser light. This optical manipulation allows only the reflection signal of the other FBG with overlapping signal to be detected and demodulated. As the shaded FBG is measured during the forward or backward laser scan, our approach can demodulate all FBGs while preventing complete signal loss. In addition, it is suitable for high-speed real-time measurements because overlapping can be solved by simply adjusting the FSW operation without complex signal processing.

Buffered FDML lasers with multiple wavelength sweeps can achieve a very high measurement rate. On the other hand, the number of detected reflection signals of FBGs can increase by several times compared with that of a typical laser, increasing the possibility of signal overlapping, especially in high-density FBG setups. Our measurement system suppresses signal overlapping in the buffered FDML laser to enable flexible high-speed FBG measurements. We demonstrate that the proposed measurement system with a three-buffered FDML laser allows the installation of FBGs at arbitrary distances and can measure strain and vibration with overlapping correction.

2 Experimental Setup

2.1 *FBG Measurement System*

Figure 1 shows the proposed measurement system using a three-buffered FDML laser. The three-buffered FDML laser consists of an FDML laser, an optical amplifier, an FSW, and a buffer stage

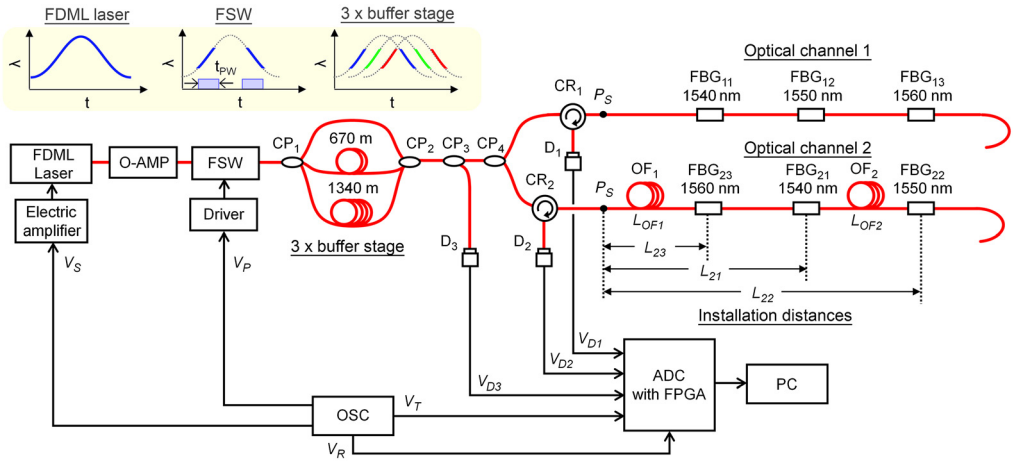

Fig. 1 FBG measurement system with three-buffered FDML laser. O-AMP, optical amplifier; FSW, fiber switch; CP, coupler; CR, circulator; Ps, reference position; OF, offset fiber; D, detector; OSC, oscillator; ADC, analog-to-digital converter; FPGA, field-programmable gate array; PC, personal computer; V_S, sweep control signal; V_P, pulse control signal; V_T, trigger signal; and V_R, reference clock signal.

with three optical paths. The FDML laser is a ring-cavity laser that uses a fiber Fabry–Perot tunable filter (FFP-TF, Micron Optics).[28,33] The laser is controlled by a sweep signal (V_S) from the oscillator (33612A, Agilent) and operates at sweep rate $f_m = 50.7$ kHz and sweep bandwidth $\Delta\lambda = 60$ nm. The FDML laser sinusoidally sweeps the oscillation wavelength from short to long wavelengths (forward scan) and from long to short wavelengths (backward scan). The optical amplifier (SOA1013, Thorlabs) magnifies the light emitted by the FDML laser. The amplified light is injected into an FSW (NSSW, Agiltron) with a rise/fall time of 100 ns. The sweep control signal V_S and pulse control signal V_P for the FDML laser are controlled by the oscillator having two channels, and the two signals are output synchronously. The FFP-TF and most of the optical fibers that make up the FDML laser are set at a constant temperature of 25°C using a thermal chamber (SLC-25A, Mitsubishi Electric Engineering).[28]

During measurement using the buffered FDML laser, the FSW is controlled by V_P with oscillator pulse width (PW) $t_{\mathrm{PW}} \approx 3\ \mu$s ($\sim 1/6f_m$), as shown in Fig. 1, to extract light in the center wavelength region of the forward and backward scans. The extracted light enters the buffer stage that is branched into three optical paths. The buffer stage has delay fibers of 670 and 1340 m with delays of 3.3 ($1/6f_m$) and 6.6 μs ($2/6f_m$), respectively. Thus, when the light extracted by the FSW is injected into the buffer stage, triple-multiplexed light in the forward and backward scans is generated owing to the delays between the optical paths.

The measurement system uses bidirectional forward and backward scans of the FDML laser with sweep rate $f_m = 50.7$ kHz to obtain a measurement rate of 101.4 kHz ($2f_m$). The measurement system then performs a triple-multiplexed wavelength sweep using the triple-buffer stage to increase the measurement rate to 304.2 kHz ($6f_m$). For identification of overlapping FBG signals, the measurement system adjusts the FSW as detailed in Sec. 2.2.

The emitted light from the three-buffered FDML laser is split by a coupler and enters optical channel $K(=1,2)$ connected to an FBG sensor. $\mathrm{FBG_{KJ}}$ ($J = 1,2,3$) has Bragg wavelength λ_{KJ} of 1540, 1550, and 1560 nm, respectively, with reflectance of ~80% and half-width of ~0.2 nm. $\mathrm{FBG_{1}}_J$ in optical channel 1 is installed in a general wavelength order, while $\mathrm{FBG_{2}}_J$ in optical channel 2 can be installed at an arbitrary position. This verifies that the proposed system can handle both general and arbitrary installations for measurement. Offset fibers with lengths L_{OF1} and L_{OF2} are inserted in front of $\mathrm{FBG_{23}}$ and $\mathrm{FBG_{22}}$, respectively, such that they can be placed at arbitrary installation distances. Reference position P_S is the distance corresponding to the fiber length at which the wavelength sweep characteristics of the laser are measured. Therefore, when the installation position of the FBG exceeds reference position P_S, a delay occurs owing to the propagation time of the optical fiber.[28,33] Installation distances L_{KJ} for each $\mathrm{FBG_{KJ}}$ are given in Table 1.

Table 1 Installation distance of each FBG.

Optical channel K	FBG_{KJ}	Bragg wavelength λ_{KJ} (nm)	Installation distance L_{KJ} (m)
1	FBG_{11}	1540	4.23
	FBG_{12}	1550	7.54
	FBG_{13}	1560	11.95
2	FBG_{21}	1540	$10.75 + L_{OF1}$
	FBG_{22}	1550	$16.32 + L_{OF1} + L_{OF2}$
	FBG_{23}	1560	$5.12 + L_{OF1}$

The reflected light of the FBGs from each optical channel is received by the corresponding detector (D_K), and the detector signals (V_{DK}) are input to an analog-to-digital converter (ADC). Detector D_3 receives the optical output of the buffered FDML laser, and detector signal V_{D3} is input to the converter (5170R, NI), which has a field-programmable gate array (FPGA) with a sampling frequency of 250 MHz to calculate the peak times of the FBG reflection signals from V_{D1} and V_{D2} and transfer them to a computer.[36] The computer converts the peak time into a reflection wavelength based on the wavelength sweep characteristics of the laser. In experiments, pulse modulation of the FSW is used to identify the reflection signal of each FBG and handle the overlapping, and the reflection wavelength of each FBG is measured at a rate of 304.2 kHz.

The measurement system is implemented in the NI LabVIEW programming language. Figure 2 shows a screenshot of the measurement system interface. The system uses signal

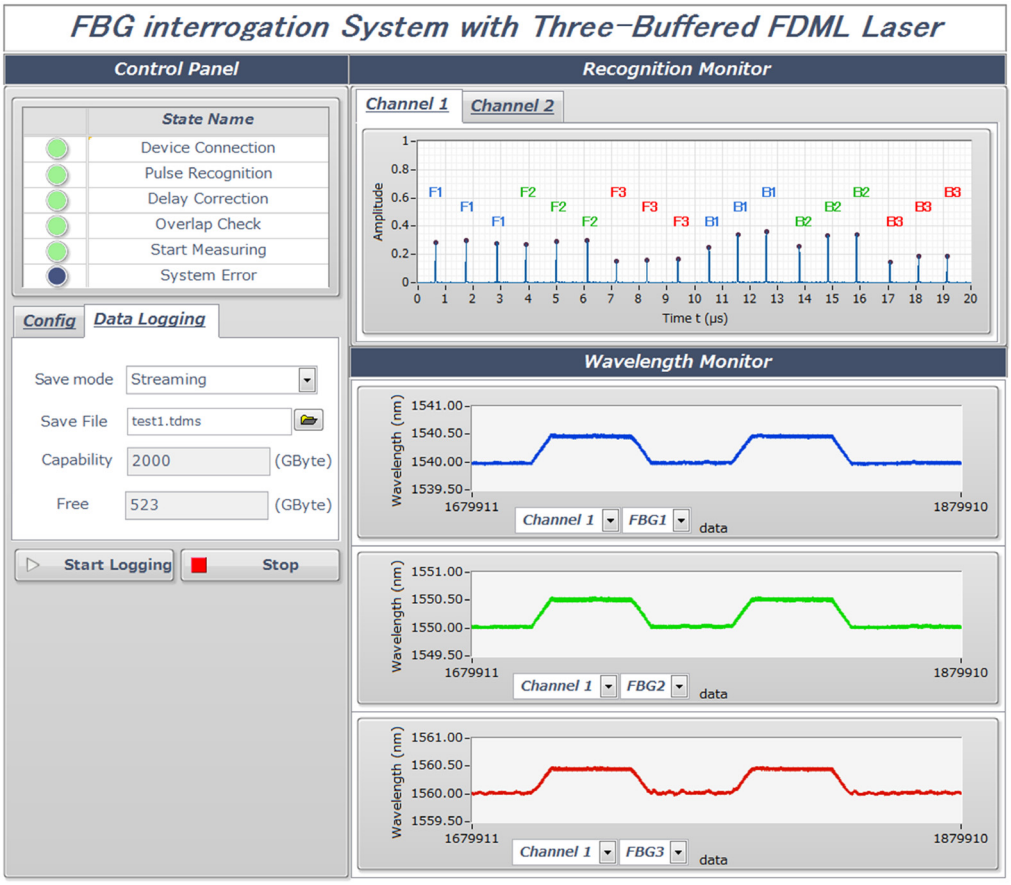

Fig. 2 Screenshot of FBG measurement system interface.

processing to identify and delay-correct the reflection signal of each FBG per optical channel. After detecting overlapping, real-time measurement begins. The data volume of the peak wavelengths of all the FBGs measured by the system is ∼14.6 MB/s, which can be stored in a commercially available external hard disk drive. The proposed measurement system allows real-time observation and recording of wavelength changes caused by strain and vibration in each FBG per optical channel.

2.2 *Signal Processing for Overlapping FBG Signals*

Figure 3 shows the signal processing flow of the proposed measurement system. The system first uses pulse modulation of the laser to identify the reflection signal of each FBG.[38] This process adjusts PW t_{PW} of the optical FSW to ∼1 μs and extracts only light in the wavelength region of a specific FBG per forward and backward scan. Hence, only FBG reflection signals at specific wavelengths are extracted and identified per scan. As the buffered FDML laser has a triple-wavelength sweep, three reflection signals can be detected and identified simultaneously. This process is performed for every FBG, completing signal identification for all the FBGs [Fig. 3(a)].

To compensate for delays owing to the FBG position, we use bidirectional scan for the wavelength-swept laser. Light in the wavelength region of a specific FBG is simultaneously extracted by the FSW in both the forward and backward scans. This operation allows the delay to be corrected by obtaining time difference t_D between the reflection signals by the forward and backward scans [Fig. 3(b)].[33,38]

The detection status of the reflection signal of each FBG per scan can then be checked. Hence, it is easy to determine close FBG reflection signals that cause overlapping depending on the FBG installation position and wavelength. We set the occupied wavelength band of each FBG to 3 nm. The decision process identifies overlapping when the reflection signals of the FBGs are closer than 3 nm. In our laser, a wavelength change of 3 nm corresponds to a time variation of ∼0.3 μs. Therefore, an overlap is determined when two reflection signals occur within ∼0.3 μs.

If overlapping is not detected, the laser light is emitted at $t_{PW} \approx 3$ μs and the reflection signals of the FBGs are detected [Fig. 3(c)]. On the other hand, if the signals overlap, the light in the wavelength region of one overlapping FBG is shaded from the wavelength-swept laser light with shading width $t_{PL} \approx 1$ μs [Fig. 3(d)]. As a result, the reflection signals of one overlapping FBG are suppressed, and those of the other overlapping FBG can be demodulated. The shaded FBG can be demodulated by either forward or backward scanning of the buffered FDML laser. This completes the signal processing shown in Fig. 3 of the measurement system, and real-time measurements can begin afterward.

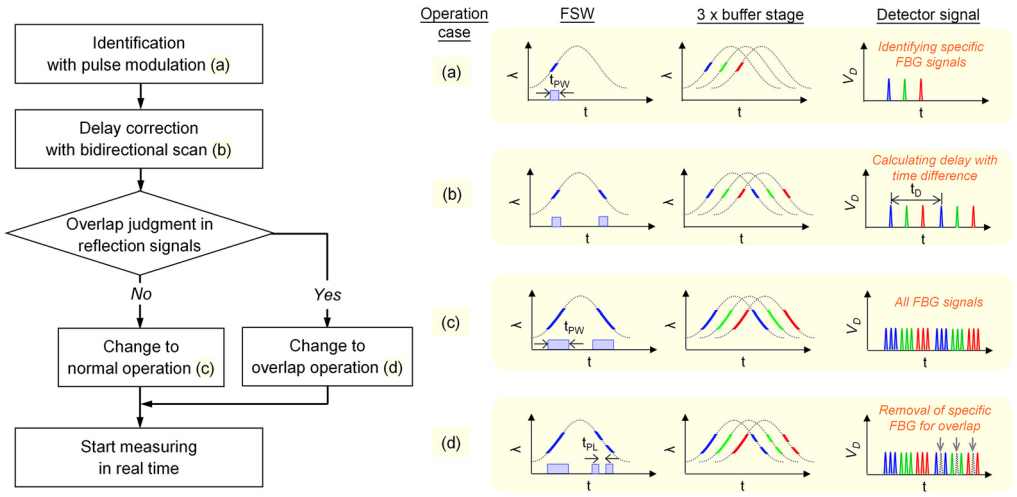

Fig. 3 Signal processing flow for overlapping FBG reflection signals.

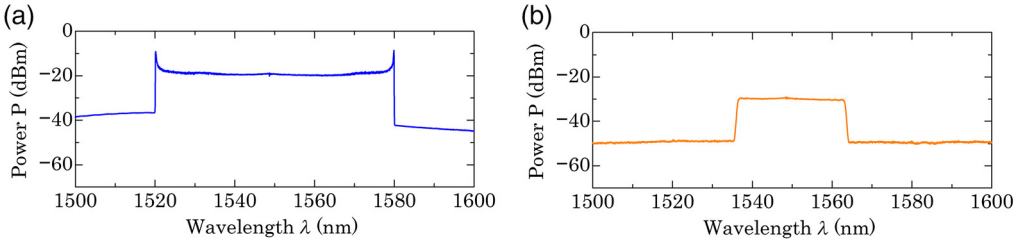

Fig. 4 Output spectrum of (a) FDML laser and (b) three-buffered FDML laser.

3 Experimental Results

3.1 *Characteristics of Three-Buffered FDML Laser*

Figures 4(a) and 4(b) show the output spectrum of the FDML and the three-buffered FDML lasers. The optical output was measured using an optical spectrum analyzer with a time average of 10. The FDML laser was driven at sweep rate $f_m = 50.7$kHz with a center wavelength of 1550 nm and a sweep bandwidth of ∼60 nm. The buffered FDML laser extracted light in the central wavelength region of the FDML laser using the FSW, as shown in Fig. 1. The extracted light was then injected into the buffer stage with three optical paths to attempt triple multiplexing of the wavelength sweep. Therefore, the buffered FDML laser had an optical output with a center wavelength of 1550 nm and a sweep bandwidth of ∼28 nm.

Next, the wavelength sweep characteristics of the buffered FDML laser were evaluated by an optical system using a wavelength monitor.[33] Figure 5 shows the results of the sweep characteristics of the buffered FDML laser for sweep period $T_m = 19.7$ μs $(1/f_m)$. Six sweeps of triple forward scans ($F1$, $F2$, and $F3$) and triple backward scans ($B1$, $B2$, and $B3$) were obtained by the buffer stage with three optical paths. Therefore, a measurement rate of 304.2 kHz $(6f_m)$ was achieved when measuring the reflection wavelength of the FBG. The measurement system performed signal processing as shown in Fig. 3 to determine overlapping. Then, using the sweep characteristics of the buffered FDML laser shown in Fig. 5, the reflection wavelength was converted from the time of the FBG reflection signal to the reflection wavelength, and real-time measurements were performed. The FDML laser sweeps the oscillation wavelength in a sinusoidal manner. This system measures the wavelength sweep characteristics in advance using a wavelength monitor and applies an eighth-order polynomial approximation to the sinusoidal waveform in each sweep scan. In the experiment, the obtained polynomial approximations are used to convert the FBG reflection signals from time to wavelength.

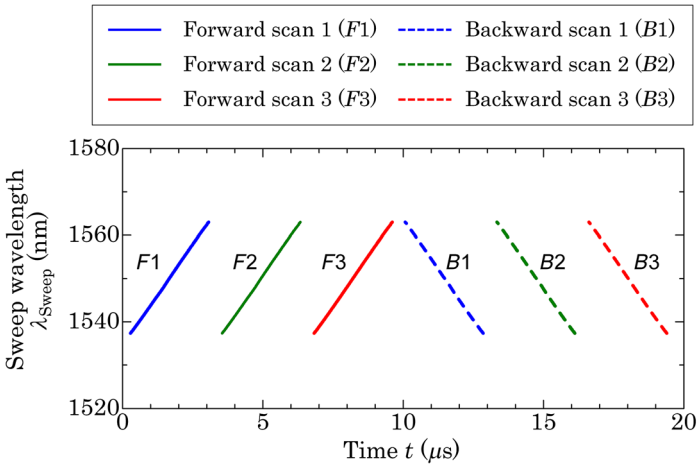

Fig. 5 Sweep characteristics of three-buffered FDML laser.

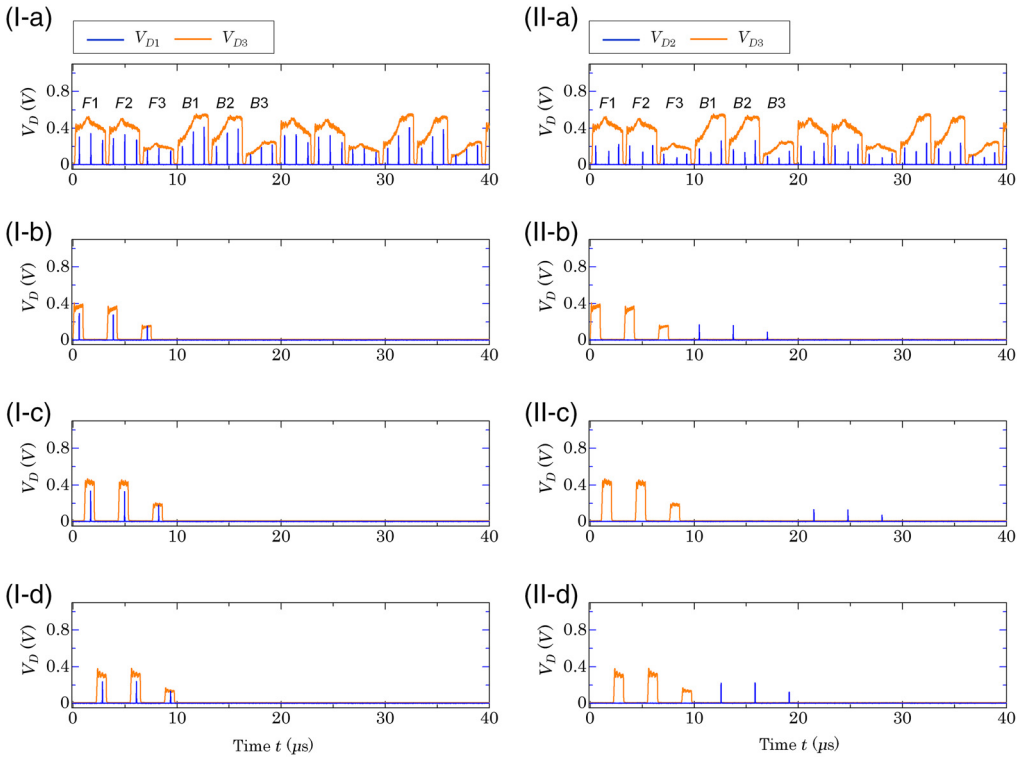

Fig. 6 Reflection signals of FBGs at $L_{OF1} = 1000$ m and $L_{OF2} = 1000$ m (I-a) with three-buffered FDML laser for optical channel 1 and identification for (I-b) FBG_{11}; (I-c) FBG_{12}; and (I-d) FBG_{13}. Reflection signals (II-a) with three-buffered FDML laser for optical channel 2 and identification for (II-b) FBG_{21}; (II-c) FBG_{22}; and (II-d) FBG_{23}. Three forward scans are $F1$, $F2$, and $F3$ respectively; three backward scans are $B1$, $B2$, and $B3$ respectively.

3.2 *Identification and Correction of Overlapping FBG Signals*

Figures 6(I) and 6(II) show the FBG reflection signals in optical channels 1 and 2, respectively. The offset fibers for optical channel 2 were set to $L_{OF1} = 1000$ m and $L_{OF2} = 1000$ m. Figures 6(I-a) and 6(II-a) show the results from the buffered FDML laser with PW $t_{PW} \asymp 3$ μs. The buffered FDML laser provided six optical pulses in forward scans ($F1, F2$, and $F3$) and backward scans ($B1, B2$, and $B3$). The time interval of the pulses was 3.3 μs ($1/6f_m$). Optical channel 1 corresponded to a general FBG installation, where each FBG was installed in order of wavelength and short distance, as given in Table 1. Therefore, the order of detection of the reflection signals of the FBGs was easily identified. Eighteen reflection signals were detected in three FBGs over six sweeps. On the other hand, as optical channel 2 was set in an arbitrary wavelength order and the installation distance was substantially different across FBGs, the detection order of the FBG reflection signals was difficult to determine.

Identification using pulse modulation was performed in the forward scan of the buffered FDML laser. The pulse width was adjusted to $t_{PW} \approx 1$ μs. Figures 6(I-b)–6(I-d) show the identification results for FBG_{11}, FBG_{12}, and FBG_{13}, respectively, and optical channel 1. Figures 6(II-b)–6(II-d) show the identification results for FBG_{21}, FBG_{22}, and FBG_{23}, respectively, and optical channel 2. By using pulse modulation, only the reflection signals of specific FBGs in forward scans ($F1, F2$, and $F3$) were extracted. In optical channel 2, where the offset fibers were installed, the reflection signals had delays because of distant FBGs. The reflection signals of FBG_{12} in optical channel 1 were $t_{\tau\_12}^{(F1)} = 1.70$ μs, $t_{\tau\_12}^{(F2)} = 4.96$ μs, and $t_{\tau\_12}^{(F3)} = 8.24$ μs. The reflection signals of FBG_{22} in optical channel 2 were $t_{\tau\_22}^{(F1)} = 21.50$ μs, $t_{\tau\_22}^{(F2)} = 24.77$ μs, and $t_{\tau\_22}^{(F3)} = 28.05$ μs. Thus, FBG_{22} was delayed with respect to FBG_{12} by $\sim$19.8 μs owing to $L_{OF1} = 1000$ m and $L_{OF2} = 1000$ m. This delay was equal to one cycle of a sweep period (T_m). FBG_{21} and FBG_{23} were delayed with respect to FBG_{11} and FBG_{13} by $\sim$9.9 μs, being half of a

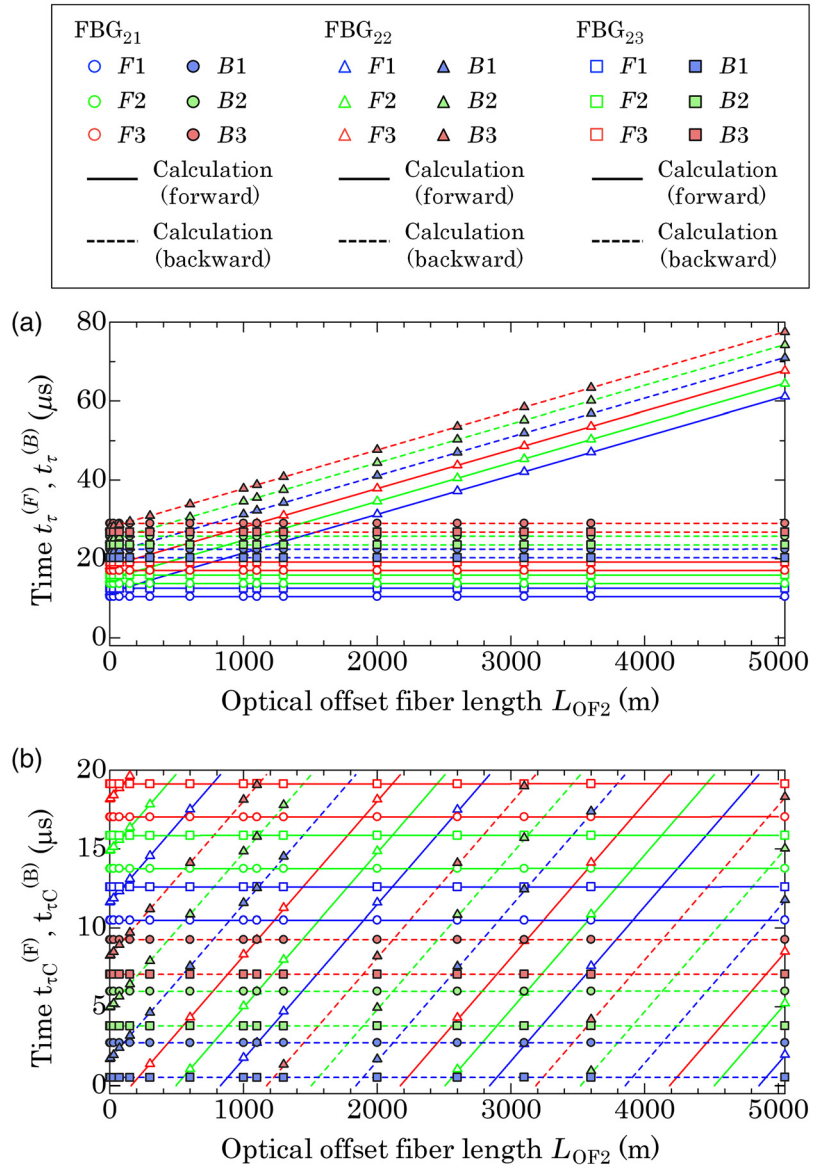

Fig. 7 Reflection signals by optical offset fiber L_{OF2}. (a) Reflection time with pulse modulation of three-buffered FDML laser. (b) Reflection time folded back at a sweep period.

sweep period ($T_m/2$) owing to $L_{OF1} = 1000$ m. Identification by pulse modulation was also performed for the backward scan of the buffered FDML laser, confirming the identification of individual FBG reflection signals.

Next, to examine in detail the identification by using pulse modulation, length L_{OF2} was changed and the FBG reflection signal in optical channel 2 was measured. Figure 7(a) shows the FBG reflection signal according to L_{OF2}. The FBG reflection signal per scan was identifiable even when L_{OF2} varied. The reflection signals of FBG_{21} and FBG_{23} were constant because they were insensitive to L_{OF2}. The reflection signals of FBG_{22} varied proportionally to L_{OF2}, with a time variation of 9.8 ns per unit length variation of L_{OF2}. This was consistent with the propagation time per unit length of the optical fiber. These results indicate that pulse modulation allows to identify installations with arbitrary wavelength order over a wide range from 0 to 5050 m by using L_{OF2}, confirming its effectiveness for arbitrary installation of FBGs.

When real-time measurements are acquired using the buffered FDML laser for a distant FBG, a reflection signal is folded back to a sweep period of 19.7 μs ($1/f_m$).[38] Therefore, we folded the results in Fig. 7(a) back over the sweep period, obtaining the results shown in Fig. 7(b). The FBG

reflection signals folded back due to the change in L_{OF2}, and their change suitably agreed with the calculated value by the optical fiber length, indicating that our process is effective for identification at the time of folding. Therefore, during real-time measurement, this process can easily identify the detection order for reflection signal measurement. In Fig. 6(II-a) ($L_{OF2} = 1000$ m), the detection order is $[t^{(B1)}_{\tau C\_23}, t^{(F1)}_{\tau C\_22}, t^{(B1)}_{\tau C\_21}, t^{(B2)}_{\tau C\_23}, t^{(F2)}_{\tau C\_22}, t^{(B2)}_{\tau C\_21}, t^{(B3)}_{\tau C\_23}, t^{(F3)}_{\tau C\_22}, t^{(B3)}_{\tau C\_21}, t^{(F1)}_{\tau C\_21}, t^{(B1)}_{\tau C\_22}, t^{(F1)}_{\tau C\_23}, t^{(F2)}_{\tau C\_21}, t^{(B2)}_{\tau C\_22}, t^{(F2)}_{\tau C\_23}, t^{(F3)}_{\tau C\_21}, t^{(B3)}_{\tau C\_22}, t^{(F3)}_{\tau C\_23}]$ according to the results shown in Fig. 7(b). The reflection signal of each FBG was measured with both forward and backward scans. Therefore, in the reflection wavelength measurements of the FBG, the delay was corrected by determining the time difference between the FBG reflection signals obtained from the scans.[33,38]

Depending on length L_{OF2}, FBG reflection signals closer than 0.3 μs occurred. Consequently, the 3-nm occupied wavelength range of the FBG could not be secured, causing overlapping reflection signals. At $L_{OF2} = 1100$ m, overlapping occurred at six locations corresponding to $[t^{(F1)}_{\tau C\_22}, t^{(B1)}_{\tau C\_21}]$, $[t^{(F2)}_{\tau C\_22}, t^{(B2)}_{\tau C\_21}]$, $[t^{(F3)}_{\tau C\_22}, t^{(B3)}_{\tau C\_21}]$, $[t^{(B1)}_{\tau C\_22}, t^{(F1)}_{\tau C\_23}]$, $[t^{(B2)}_{\tau C\_22}, t^{(F2)}_{\tau C\_23}]$, and $[t^{(B3)}_{\tau C\_22}, t^{(F3)}_{\tau C\_23}]$. Thus, pulse modulation allowed to identify both the FBG reflection signals and the overlapping sources.

The proposed measurement system implements an alert function to visualize overlapping based on identification by pulse modulation (Fig. 8). The occurrence of an alert is determined by the degree of proximity of the FBG reflection signals owing to pulse modulation. Therefore, when the system obtains a result for optical channel 2 with $L_{OF2} = 1100$ m, it automatically generates six alerts. The system also displays the alert source, with alert 1 (around 2.7 μs) indicating the occurrence of overlapping at $[t^{(F1)}_{\tau C\_22}, t^{(B1)}_{\tau C\_21}]$.

Figure 9 shows the reflection signals when alert 1 shown in Fig. 8 occurs. In Fig. 9(a), the reflection signals of $t^{(F1)}_{\tau C\_22}$ and $t^{(B1)}_{\tau C\_21}$ overlap, hindering their separation and demodulation. Figs. 9(b)–9(d) show the results of applying strain $\Delta\varepsilon_{22} = 100, 200$, and 300 $\mu\varepsilon$ to FBG_{22}, respectively. With the application of strain, reflection signals $t^{(F1)}_{\tau C\_22}$ of FBG_{22} were gradually separated.

As a slight change by strain or vibration can cause signal separation and assimilation, overlapping FBG reflection signals are difficult to demodulate in measurement systems. Therefore, the signal processing in Fig. 3, which shades a specific FBG, was implemented to solve overlapping. To prevent the occurrence of the six overlapping regions in Fig. 8, the FBGs must be shaded in any of the three switch patterns detailed in Table 2. Switch pattern SP1 shaded all backward scans ($B1, B2$, and $B3$) in the wavelength region of FBG_{21}, eliminating alerts 1–3 shown in Fig. 8. In the buffered FDML laser, even if only $B1$ of the backward scan was shaded, B2 and B3 were also simultaneously shaded owing to triple multiplexing, thus shading all backward scans. In switch pattern SP1, all forward scans ($F1, F2$, and $F3$) in the wavelength region of FBG_{23} were also shaded to eliminate alerts 4–6.

Figure 10 shows the results of measuring the FBG reflection signals for each switch pattern indicated in Table 2. FBG_{22} was set at strain $\Delta\varepsilon_{22} = 200$ $\mu\varepsilon$. Figure 10(I-a) shows reflection signals for $L_{OF2} = 1100$ m. Reflection signals overlapped in the time domain according to the

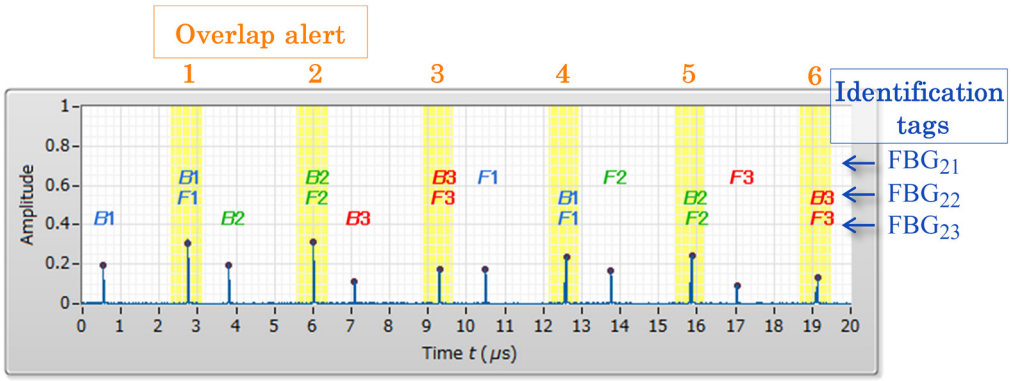

Fig. 8 Screenshot showing overlap alerts ($L_{OF2} = 1100$ m).

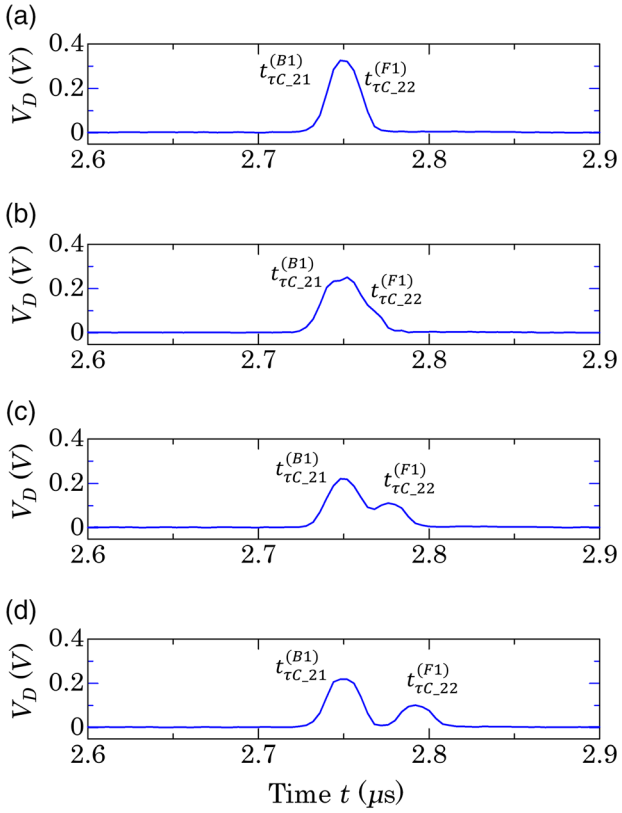

Fig. 9 Results of reflection signals when alert 1 occurs for $L_{OF2} = 1100$ m under applied strain $\Delta\varepsilon_{22}$ of (a) 0; (b) 100; (c) 200; and (d) 300 $\mu\varepsilon$.

Table 2 Switch pattern for measuring overlapping FBG reflection signals at $L_{OF2} = 1100$ m.

FBG	FBG_{21}		FBG_{22}		FBG_{23}	
Wavelength (nm)	1540		1550		1560	
F/B	F	B	F	B	F	B
SP1	○	↓	○	○	⇓	○
SP2	○	○	↓	○	⇓	○
SP3	○	↓	○	⇓	○	○

Note: F: forward scan; B: backward scan; ○: switch on; and ↓, ⇓: switch off.

six alerts shown in Fig. 8. Figures 10(I-b) and 10(I-c) show the magnified views in the periods where alerts 1 and 4 occurred. In both regions, reflection signals of two FBGs were close.

Figures 10(II)–10(IV) show the results of shading specific FBGs for switch patterns SP1, SP2, and SP3 (Table 2), respectively. In Fig. 10(II-a) for switch pattern SP1, all backward scans ($B1$, $B2$, and $B3$) in the wavelength region of FBG_{21} were shaded. Therefore, in Fig. 10(II-b) of alert 1, $t_{\tau C\_21}^{(B1)}$ was removed and only the $t_{\tau C\_22}^{(F1)}$ was detected. In Fig. 10(II-a), all forward scans ($F1$, $F2$, and $F3$) in the wavelength region of FBG_{23} were shaded. In Fig. 10(II-c) of alert 4, $t_{\tau C\_23}^{(F1)}$ was removed and only $t_{\tau C\_22}^{(B1)}$ was detected. The processing of switch pattern SP1 confirmed that the reflection signals of one FBG was removed in the results of other alerts as well as in the results of alerts 1 and 4. By changing the FBG for shading with switch patterns, as shown in Figs. 10(III) and 10(IV), the reflection signal of the desired FBG could be shaded and

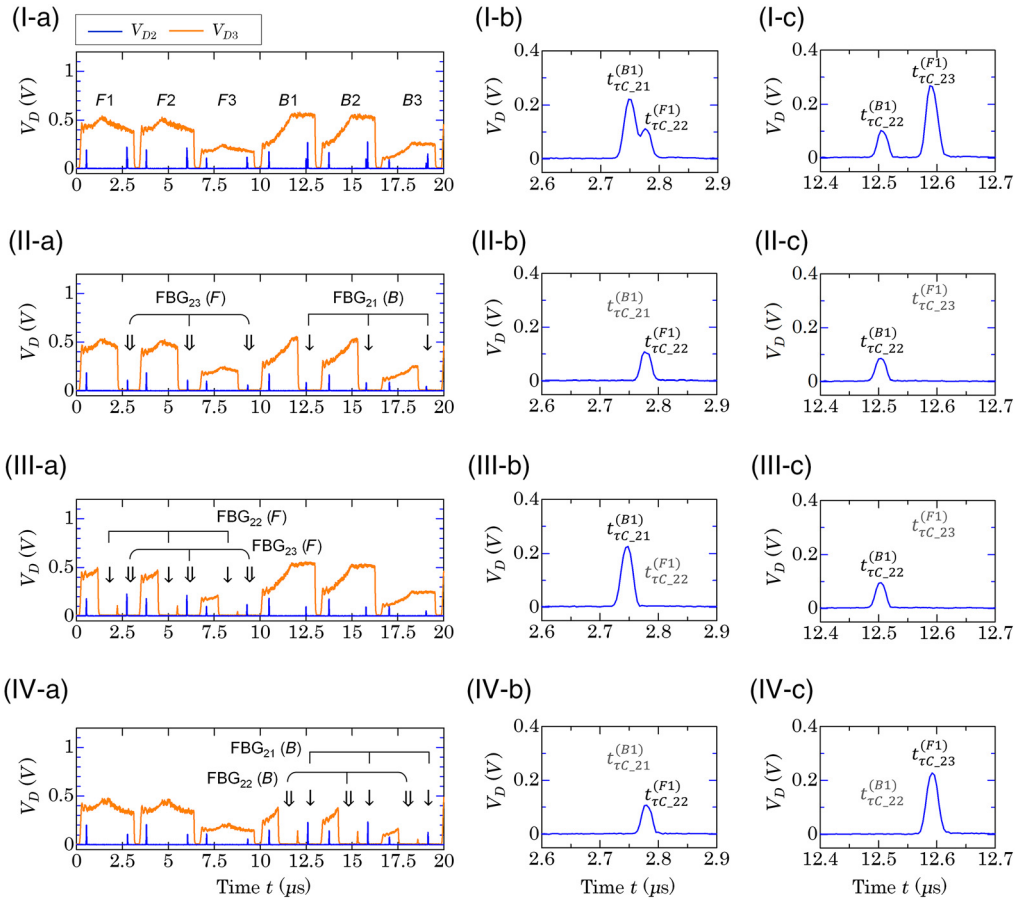

Fig. 10 Reflection signals with overlapping at $L_{OF2} = 1100$ m (I) with three-buffered FDML laser and switch patterns (II) SP1; (III) SP2; and (IV) SP3 for overlapping. (a) Reflection signals and their magnified views around; (b) 2.7 μs (alert 1); and (c) 12.5 μs (alert 4).

acquired. By adjusting the switch pattern, only one FBG with overlapping reflection signals could be detected, thus suppressing overlapping.

3.3 *FBG Measurements with Measurement System*

Strain measurements were performed using FBGs with multiple optical channels. To generate strain, one end of an optical fiber of length $L = 1$ m containing an FBG was attached to a fixed stage, and the other end was attached to a movable stage (SGSP26-100, SIGMAKOKI). The movable stage was moved along the longitudinal direction of the optical fiber by variation ΔX to stretch the optical fiber, and strain $\Delta\varepsilon(= \Delta X/L)$ was applied. To verify the effect of identification and delay correction for FBGs in this experimental setup, $L_{OF1} = 1000$ m was fixed and L_{OF2} was set to 0, 2000, and 5050 m. The length conditions did not cause overlapping reflection signals between the FBGs. Figure 11 shows the strain measurements for each FBG and optical channel. The reflection wavelength of each FBG changed to longer wavelengths in proportion to the strain. The slope of the reflection wavelength with respect to strain was 1.2×10^{-3} nm/$\mu\varepsilon$ per FBG. Almost identical reflection wavelengths were obtained even for varying delays owing to the installation distance via L_{OF2}. The difference between the measured values at L_{OF2} of 2000 and 5050 m with L_{OF2} of 0 m was below 5×10^{-2} nm for all FBGs. The standard deviation of the reflection wavelength per FBG and optical channel was <9 pm. These results indicate that the proposed measurement system with the three-buffered FDML laser identifies and corrects the delay of multiple FBG reflection signals and enables multichannel strain measurements with FBGs over a wide installation range from 0 to 5050 m.

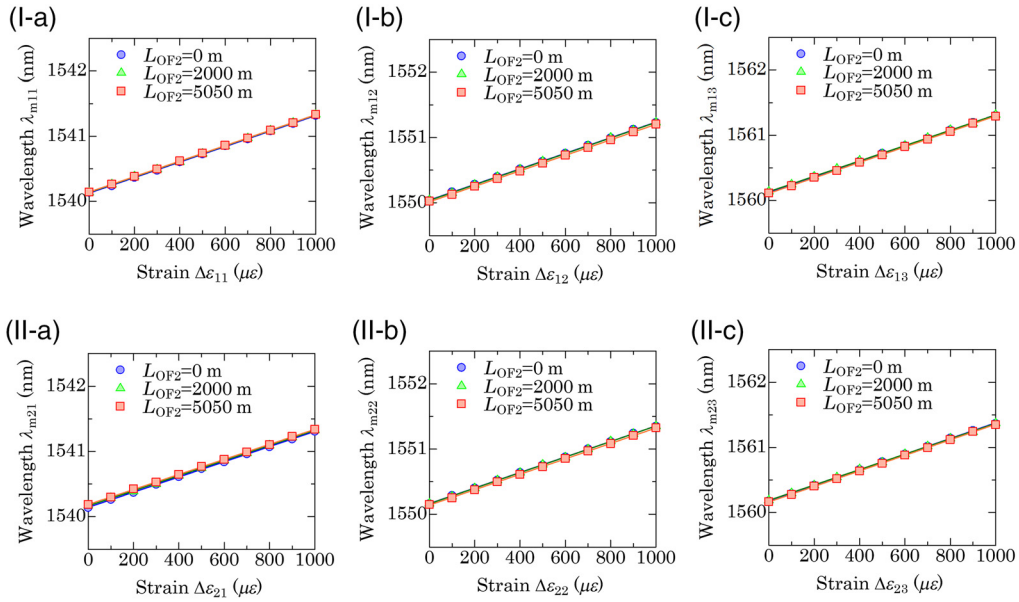

Fig. 11 Strain measurements for each FBG and optical channels (I) 1 and (II) 2. Measurements for (I-a) FBG_{11}; (I-b) FBG_{12}; (I-c) FBG_{13}; (II-a) FBG_{21}; (II-b) FBG_{22}; and (II-c) FBG_{23}.

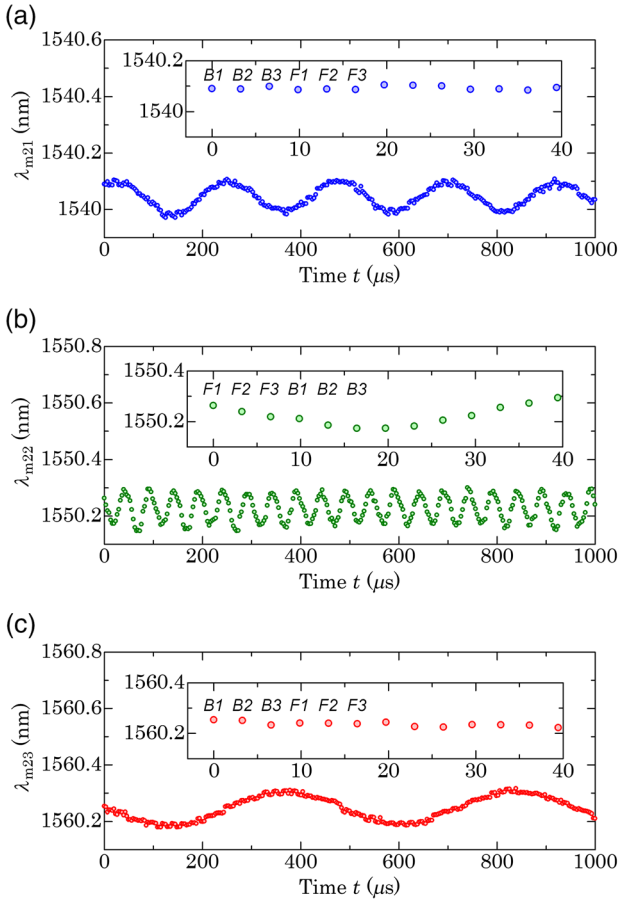

Fig. 12 Vibration measurements without overlapping for $L_{OF2} = 1000$ m in (a) FBG_{21}; (b) FBG_{22}; and (c) FBG_{23}.

Real-time vibration measurements were also performed using FBGs in optical channel 2. FBG_{21} and FBG_{23} were attached to bimorph piezoelectric transducers with vibration frequencies $f_{V21} = 4.46$ kHz and $f_{V23} = 2.12$ kHz, respectively. FBG_{22} vibrated through a metal-shielded piezoelectric actuator with vibration frequency $f_{V22} = 20$ kHz. This experiment was conducted at L_{OF2} of 1000 m without overlapping and 1100 m with overlapping. Figure 12 shows the vibration measurements without overlapping ($L_{OF2} = 1000$ m). Figures 12(a)–12(c) show the results for FBG_{21}, FBG_{22}, and FBG_{23}, respectively. The reflection wavelength of each FBG changed at each applied vibration frequency. The peak-to-peak values of the reflection wavelengths due to the vibration of each FBG were ~0.13, 0.15, and 0.13 nm, respectively. Without overlapping, as shown in Fig. 7(b), all reflection signals of each FBG were detected in the six forward and backward scans without signal proximity. In addition, the reflection wavelengths were calculated according to the order of detection of the FBG reflection signals identified by pulse modulation. The order of reflection wavelengths for FBG_{21} was $[t_{\tau C\_21}^{(B1)}, t_{\tau C\_21}^{(B2)}, t_{\tau C\_21}^{(B3)}, t_{\tau C\_21}^{(F1)}, t_{\tau C\_21}^{(F2)}, t_{\tau C\_21}^{(F3)}]$. The proposed measurement system using the three-buffered FDML laser achieved a time resolution of 3.3μs $(1/6f_m)$.

The offset fiber was then changed to $L_{OF2} = 1100$ m, obtaining the vibration measurements with overlapping shown in Fig. 13. Overlapping was solved by applying switch pattern SP1 (Table 2). Figures 13(a)–13(c) show the results for FBG_{21}, FBG_{22}, and FBG_{23}, respectively. By shading the wavelength region of FBG reflection signals to eliminate overlapping, the reflection wavelength of each FBG could be demodulated. Each FBG had a sinusoidal wavelength variation at each vibration frequency, as in the results without overlapping (Fig. 12). Switch pattern SP1 shaded all backward scans ($B1, B2$, and $B3$) in the wavelength region of FBG_{21} and all forward scans ($F1, F2$, and $F3$) in the wavelength region of FBG_{23} to eliminate

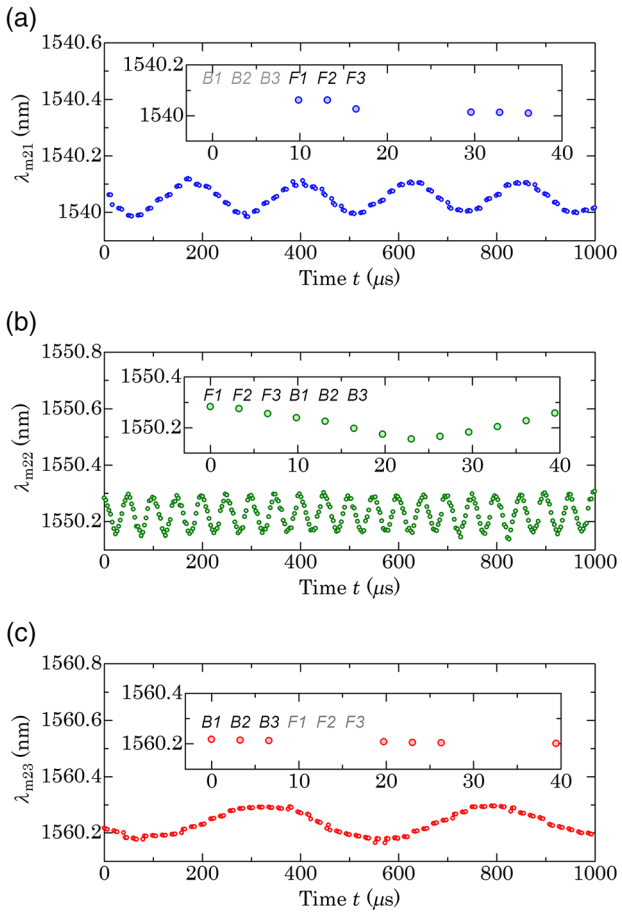

Fig. 13 Vibration measurements with overlapping for $L_{OF2} = 1100$ m in (a) FBG_{21}; (b) FBG_{22}; and (c) FBG_{23}.

overlapping. For FBG_{21} in Fig. 13(a), the unshaded forward scans ($F1, F2$, and $F3$) had the reflection wavelengths demodulated. Similarly, for FBG_{23} in Fig. 13(c), only the unshaded backward scans ($B1, B2$, and $B3$) were demodulated for the reflection wavelengths. For FBG_{22} in Fig. 13(b), no shading was applied to the forward and backward scans, and the reflection wavelengths were demodulated in both scan directions ($F1, F2, F3, B1, B2$, and $B3$). The reflection wavelengths were calculated according to the order of detection of the FBG reflection signals shown in Fig. 7(b). The peak-to-peak values of the reflection wavelengths due to vibration of each FBG were ∼0.13, 0.16, and 0.13 nm, respectively, suitably agreeing with those shown in Fig. 12. FBG_{22} measured a higher vibration frequency of 20 kHz than the other FBGs. Therefore, any switch pattern indicated in Table 2 can be used to measure FBGs, but switch pattern SP1 allows to adjust the measurement to prioritize FBG_{22}, which measures higher frequencies. Overall, these results demonstrate that shading the wavelength region of a specific FBG suppresses overlapping and enables real-time measurement of vibration with multiple FBGs.

3.4 *Considerations for Measurement Systems with Buffered FDML Lasers*

The method using buffered FDML lasers improves the measurement rate depending on the number of buffers. On the other hand, because this method involves multiplexing by extracting a portion of the wavelength-swept laser light, the sweep bandwidth is reduced. Therefore, the number of buffers should be adjusted considering the trade-off between laser sweep rate and sweep bandwidth. A two-buffered FDML laser has a sweep bandwidth of ∼39 nm, while the sweep rate is 202.8 kHz.[33] Three-buffered FDML lasers have a sweep bandwidth of ∼28 nm and a sweep rate of 304.2 kHz. The maximum number of FBGs allowed depends on the sweep bandwidth of the laser and the wavelength range occupied by the FBGs. When the occupied wavelength range of FBGs is set to 5 nm to ensure a wide strain range, the maximum number of FBGs is ∼7 and 5 for the two- and three-buffered FDML lasers, respectively. For the high-speed multichannel detection of several FBG sensors, the peak detection speed must be improved. Our system achieves real-time peak detection by designing a peak detection process using an FPGA capable of digital arithmetic and parallel processing.[36]

4 Conclusion

We introduce a measurement system that suppresses overlapping in multiple FBG reflection signals. The measurement system uses a three-buffered FDML laser with two channels, a measurement rate of 304.2 kHz and a sweep bandwidth of 28 nm. The measurement system uses laser pulse modulation to extract and identify reflection signals of FBGs placed at arbitrary distances. Furthermore, by using forward and backward laser scans, the reflection wavelength can be measured with delay compensation over a wide installation range. By identifying the reflection signals of all FBGs through pulse modulation, the overlapping signals are identified, generating an overlap alert in the system. To suppress overlapping, we shade the laser light in the wavelength region of one of the overlapping FBGs by an FSW. As a result, the measurement system suppresses reflection signal overlapping in FBGs placed at arbitrary distances and allows multichannel measurement of strain and vibration. This experiment has successfully measured the reflection wavelength of FBGs without any signal overlap. The measurement system at present prioritizes measuring all FBG wavelengths. Therefore, the measurement rate of FBGs excluded due to overlap is changing. In this regard, we will examine the possibility of frequency analysis using resampling and other techniques based on digital signal processing. In future work, we will improve the measurement system to handle higher sensor densities than the current setup.

Acknowledgments

This work was partly supported by the JSPS KAKENHI (Award No. 20K14754) and by the Nihon University College of Science and Technology for Research.

References

1. J. M. López-Higuera, *Handbook of Optical Fibre Sensing Technology*, Wiley, Hoboken, New Jersey (2002).
2. E. J. Friebele et al., "Optical fiber sensors for spacecraft applications," *Smart Mater. Struct.* **8**(6), 813–838 (1999).
3. J. M. López-Higuera et al., "Fiber optic sensors in structural health monitoring," *J. Lightwave Technol.* **29**(4), 587–608 (2011).
4. A. D. Kersey et al., "Fiber grating sensors," *J. Lightwave Technol.* **15**(8), 1442–1463 (1997).
5. A. Othonos and K. Kalli, *Fiber Bragg Gratings*, Artech House, Norwood, Massachusetts (1999).
6. K. Hotate and Z. He, "Synthesis of optical-coherence function and its applications in distributed and multiplexed optical sensing," *J. Lightwave Technol.* **24**(7), 2541–2557 (2006).
7. J. N. Caceres et al., "Spatial resolution enhancement of Brillouin optical correlation-domain reflectometry using convolutional neural network: proof of concept," *IEEE Access* **9**, 124701–124710 (2021).
8. K. Yuksel et al., "Complete analysis of multireflection and spectral-shadowing crosstalks in a quasi-distributed fiber sensor interrogated by OFDR," *IEEE Sens. J.* **12**(5), 988–995 (2012).
9. A. González-Vila et al., "Narrowband interrogation of plasmonic optical fiber biosensors based on spectral combs," *Opt. Laser Technol.* **96**, 141–146 (2017).
10. M. Zhu and H. Murayama, "Fast demodulation of OFDR based long length FBG sensing system for noisy signals," *Opt. Express* **26**(16), 19804–19814 (2018).
11. X. Liang et al., "Precision dynamic sensing with ultra-weak fiber Bragg grating arrays by wavelength to frequency transform," *J. Lightwave Technol.* **37**(14), 3526–3531 (2019).
12. Q. H. Bui et al. "Simultaneous multi-point measurement of strain and temperature utilizing Fabry-Perot interferometric sensors composed of low reflective fiber Bragg gratings in a polarization-maintaining fiber," *Opt. Express* **28**(9), 13104–13115 (2020).
13. J. Y. Sung et al., "Fiber Bragg grating sensing system with wavelength-swept-laser distribution and self-synchronization," *Opt. Lett.* **45**(19), 5436–5439 (2020).
14. N. Sonoda et al., "Multipoint bending measurement using multicore fiber Bragg grating and two-photon absorption process in Si-APD," *IEEE Sens. J.* **21**(22), 25736–25742 (2021).
15. N. Takeda et al., "Development of smart composite structures with small-diameter fiber Bragg grating sensors for damage detection: quantitative evaluation of delamination length in CFRP laminates using Lamb wave sensing," *Comp. Sci. Technol.* **65**(15–16), 2575–2587 (2005).
16. J. Y. Lee, H. Tsuda, and N. Toyama, "Impact wave and damage detections using a strain-free fiber Bragg grating ultrasonic receiver," *NDT & E Int.* **40**(1), 85–93 (2007).
17. G. Wild and S. Hinckley, "Acousto-ultrasonic optical fiber sensors: overview and state-of-the-art," *IEEE Sens. J.* **8**(7), 1184–1193 (2008).
18. H. Tsuda et al., "Acoustic emission measurement using a strain-insensitive fiber Bragg grating sensor under varying load conditions," *Opt. Lett.* **34**(19), 2942–2944 (2009).
19. Y. Zhu, Q. Sheng, and M. Han, "Effect of laser polarization on fiber Bragg grating Fabry–Perot interferometer for ultrasound detection," *IEEE Photonics J.* **12**(4), 7102408 (2020).
20. A. Navratil, J. Wee, and K. Peters, "Ultrasonic frequency response of fiber Bragg grating under direct and remote adhesive bonding configurations," *Meas. Sci. Technol.* **33**(1), 015204 (2022).
21. Q. Rong et al., "Ultrasonic imaging of seismic physical models using fiber Bragg grating Fabry–Perot probe," *IEEE J. Sel. Top. Quantum Electron.* **23**(2), 5600506 (2017).
22. S. H. Yun, D. J. Richardson, and B. Y. Kim, "Interrogation of fiber grating sensor arrays with a wavelength-swept fiber laser," *Opt. Lett.* **23**(11), 843–845 (1998).
23. T. Saitoh et al. "Ultra-long-distance fiber Bragg grating sensor system," *IEEE Photonics Technol. Lett.* **19**(20), 1616–1618 (2007).

24. R. Isago and K. Nakamura, "A high reading rate fiber Bragg grating sensor system using a high-speed swept light source based on fiber vibrations," *Meas. Sci. Technol.* **20**(3), 034021 (2009).
25. E. J. Jung et al., "Characterization of FBG sensor interrogation based on a FDML wavelength swept laser," *Opt. Express* **16**(21), 16552–16560 (2008).
26. D. Chen, C. Shu, and S. He, "Multiple fiber Bragg grating interrogation based on a spectrum-limited Fourier domain mode-locking fiber laser," *Opt. Lett.* **33**(13), 1395–1397 (2008).
27. B. C. Lee et al. "Dynamic and static strain fiber Bragg grating sensor interrogation with a 1.3 μm Fourier domain mode-locked wavelength-swept laser," *Meas. Sci. Technol.* **21**(9), 094008 (2010).
28. T. Yamaguchi and Y. Shinoda, "Real-time fiber Bragg grating measurement system using temperature-controlled Fourier domain mode locking laser," *Opt. Eng.* **56**(6), 066112 (2017).
29. R. Huber et al., "Amplified, frequency swept lasers for frequency domain reflectometry and OCT imaging: design and scaling principles," *Opt. Express* **13**(9), 3513–3528 (2005).
30. R. Huber, M. Wojtkowski, and J. G. Fujimoto, "Fourier domain mode locking (FDML): a new laser operating regime and applications for optical coherence tomography," *Opt. Express* **14**(8), 3225–3237 (2006).
31. R. Huber, D. C. Adler, and J. G. Fujimoto, "Buffered Fourier domain mode locking: unidirectional swept laser sources for optical coherence tomography imaging at 370,000 lines/s," *Opt. Lett.* **31**(20), 2975–2977 (2006).
32. J. P. Kolb et al., "High-resolution retinal swept source optical coherence tomography with an ultra-wideband Fourier-domain mode-locked laser at MHz A-scan rates," *Biomed. Opt. Express* **9**(1), 120–130 (2018).
33. T. Yamaguchi, W. Endo, and Y. Shinoda, "High-speed interrogation system for fiber Bragg gratings with buffered Fourier domain mode-locked laser," *IEEE Sens. J.* **21**(15), 16659–16669 (2021).
34. Z. Li et al., "Delay calibration method for wavelength-swept laser-based FBG demodulation system," *IEEE Photonics Technol. Lett.* **26**(20), 2082–2085 (2014).
35. J. Mei, X. Xiao, and C. Yang, "Delay compensated FBG demodulation system based on Fourier domain mode-locked lasers," *IEEE Photonics Technol. Lett.* **27**(15), 1585–1588 (2015).
36. T. Yamaguchi, K. Ishihara, and Y. Shinoda, "Field-programmable gate array-based multichannel measurement system for interrogating fiber Bragg grating sensors," *IEEE Sens. J.* **19**(15), 6163–6172 (2019).
37. X. Liang et al., "Delay-disorder fiber Bragg grating recognition and calibration method for a Fourier domain mode-locked wavelength-swept laser-based interrogation system," *Appl. Opt.* **57**(28), 8148–8153 (2018).
38. T. Yamaguchi, W. Endo, and Y. Shinoda, "Interrogation system with automatic recognition and delay correction functions of fiber Bragg gratings by pulse modulation with wavelength-swept laser," *IEEE Sens. J.* **19**(22), 10519–10528 (2019).
39. C. Z. Shi et al., "Improving the performance of a FBG sensor network using a genetic algorithm," *Sens. Actuator. A Phys.* **107**(1), 57–61 (2003).
40. J. J. Liang et al., "Wavelength detection in FBG sensor network using tree search DMS-PSO," *IEEE Photonics Technol. Lett.* **18**(12), 1305–1307 (2006).
41. H. Jiang, J. Chen, and T. Liu, "Wavelength detection in spectrally overlapped FBG sensor network using extreme learning machine," *IEEE Photonics Technol. Lett.* **26**(20), 2031–2034 (2014).
42. B. Li et al., "Dilated convolutional neural networks for fiber Bragg grating signal demodulation," *Opt. Exp.* **29**(5), 7110–7123 (2021).

Tatsuya Yamaguchi received his BS, MS, and PhD degrees in engineering from Nihon University, Tokyo, Japan, in 2013, 2015, and 2018, respectively. He then joined the Department of Electrical Engineering at Nihon University. His current research interests include optical measurements, digital signal processing, and optical fiber sensing. He is a member of the

Institute of Electrical Engineers of Japan (IEEJ), the Society of Instrument and Control Engineers (SICE), the Institute of Electrical and Electronics Engineers (IEEE), and The International Society for Optics and Photonics (SPIE).

Akira Nakamoto received his BS and MS degrees in engineering from Nihon University, Tokyo, Japan, in 2020 and 2022, respectively. He has since been employed at Nihon Kohden Corporation. His current research interest includes optical fiber sensing.

Yukitaka Shinoda received his BSc, MSc, and PhD degrees in electrical engineering from Nihon University in 1987, 1989, and 2004, respectively. He was a visiting researcher at the Virginia Polytechnic Institute and State University (Virginia Tech) from 2009 to 2010. Since 2012, he has been a professor at the College of Science and Technology, Nihon University. He has focused on laser sensing, digital signal processing, motion analysis, and optical scanning holography. He is a member of the Institute of Electrical Engineers of Japan (IEEJ), the Society of Instrument and Control Engineers (SICE), the Japan Society of Applied Physics (JSAP), and the Institute of Electrical and Electronics Engineers (IEEE).